Supporting Information

All Carbon Lithium Capacitor Based on Salt Crystals Designed N-doping Porous Carbon Electrodes with Superior Energy Storage

Yongpeng Cui, Wei Liu, Yan Lyu, Yuan Zhang, Huanlei Wang*, Yujing Liu, Dong Li*

School of Materials Science and Engineering, Ocean University of China, Qingdao 266100, China.

*Email: weiliu@ouc.edu.cn; huanleiwang@ouc.edu.cn

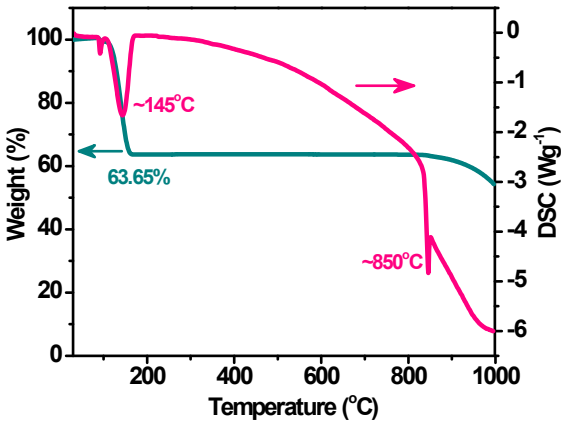

Figure S1. The TGA and DSC curves of $NaHCO_3$ under nitrogen atmosphere. There is a weight loss of 36.35% at about 145 °C, which can be ascribed to the decomposition of $NaHCO_3$ ($2NaHCO_3 \rightarrow Na_2CO_3 + H_2O + CO_2$). When the temperature is increased to about 850 °C, another weight loss is observed, indicating the Na_2CO_3 begins to decompose.

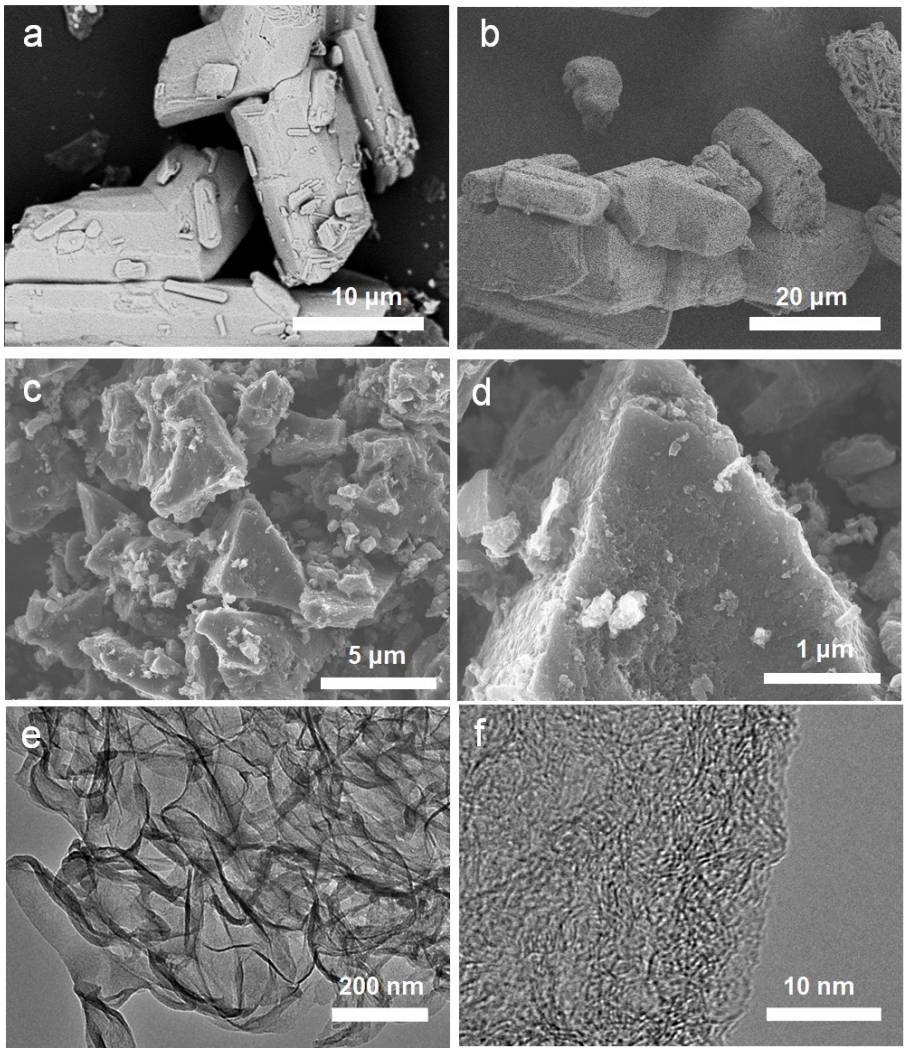

Figure S2. (a) SEM micrograph of $NaHCO_3$ crystals, (b) SEM micrograph of Na_2CO_3 framework derived from the decomposition of $NaHCO_3$ crystals at 200 ^oC. (c, d) SEM micrographs of the morphology for the NC without $NaHCO_3$ and KOH, and (e, f) TEM micrographs of the PC without adding urea. When the methyl cellulose was carbonized without activating agent, the NC displays dense and particulate-like morphology, confirming that KOH/$NaHCO_3$ plays a vital role in the formation of 3D interconnected porous structure.

Table S1. Physical and electrochemical properties of NC, PC and NPC samples.

Sample	S_{BET} [a] ($m^2\ g^{-1}$)	V_t [b] ($cm^3\ g^{-1}$)	Pore vol (%)		
			$V_{<1\ nm}$	$V_{1\text{-}2\ nm}$	$V_{>2\ nm}$
NC	616	0.43	-	-	-
PC	1771	1.98	7.5	16.5	76.5
NPC	1748	1.47	9.0	22.0	68.5

[a] Specific surface area was calculated by the Brunauer-Emmett-Teller (BET) method.

[b] Total pore volume was determined by the density functional theory (DFT) method.

Table S2. Relative surface concentrations of nitrogen and oxygen species obtained by fitting N1s and O1s core level XPS spectra.

Sample	O1s (%)			N1s (%)		
	O-I	O-II	O-III	N-6	N-5	N-Q
PC	40.82	47.21	11.97	-	-	-
NC	35.89	51.77	12.34	29.67	38.08	32.25
NPC	40.68	45.25	14.07	40.39	27.23	32.37

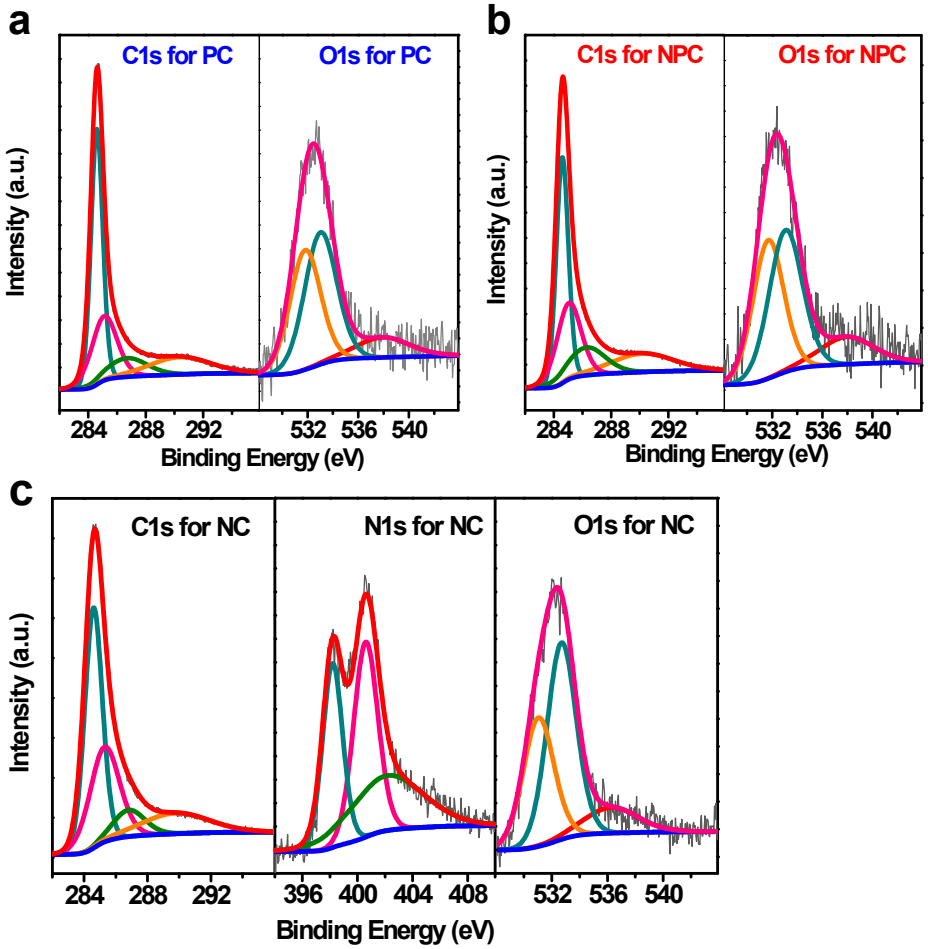

Figure S3. The high-resolution XPS C1s, N1s, and O1s spectra of (a) PC, (b) NPC, and (c) NC.

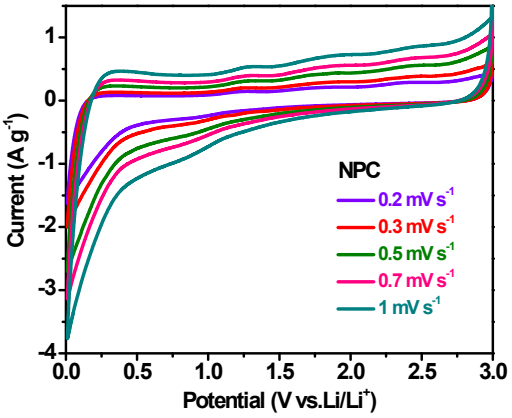

Figure S4. CV curves of the NPC electrodes at different scan rates for lithium-ion battery anodes.

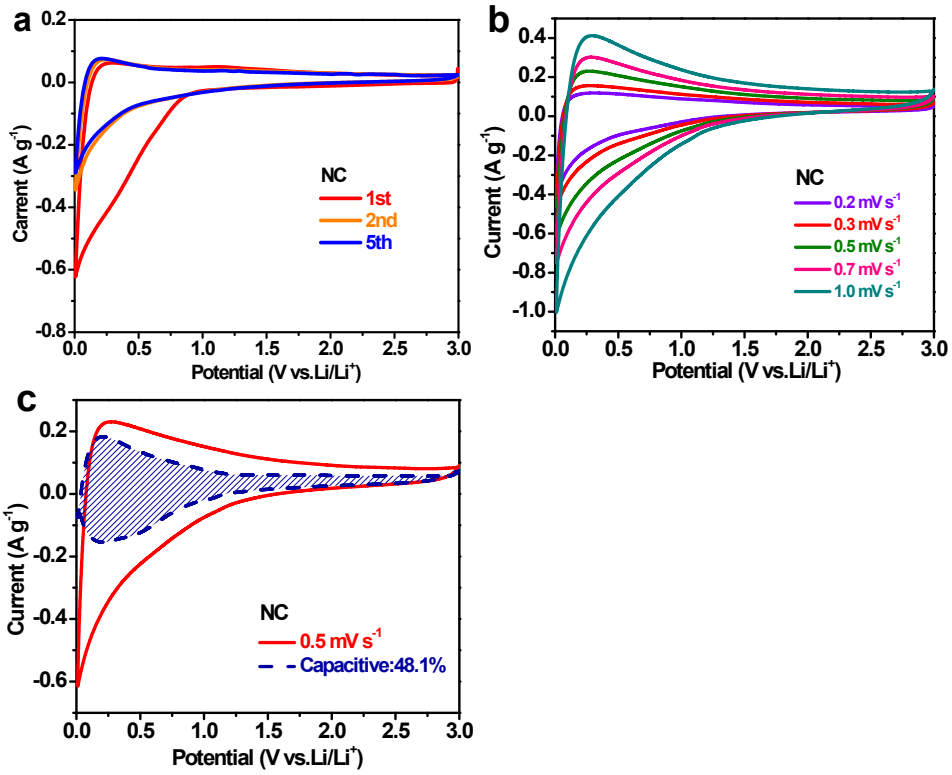

Figure S5. Electrochemical properties of NC tested for lithium-ion battery anodes. (a) CV curves for the first, second, and fifth cycles at the scan rate of 0.1 mV s^{-1}. (b) CV curve at different scan rates, and (c) CV curve at 0.5 mV s^{-1} with shadowed area representing the surface capacitive contribution.

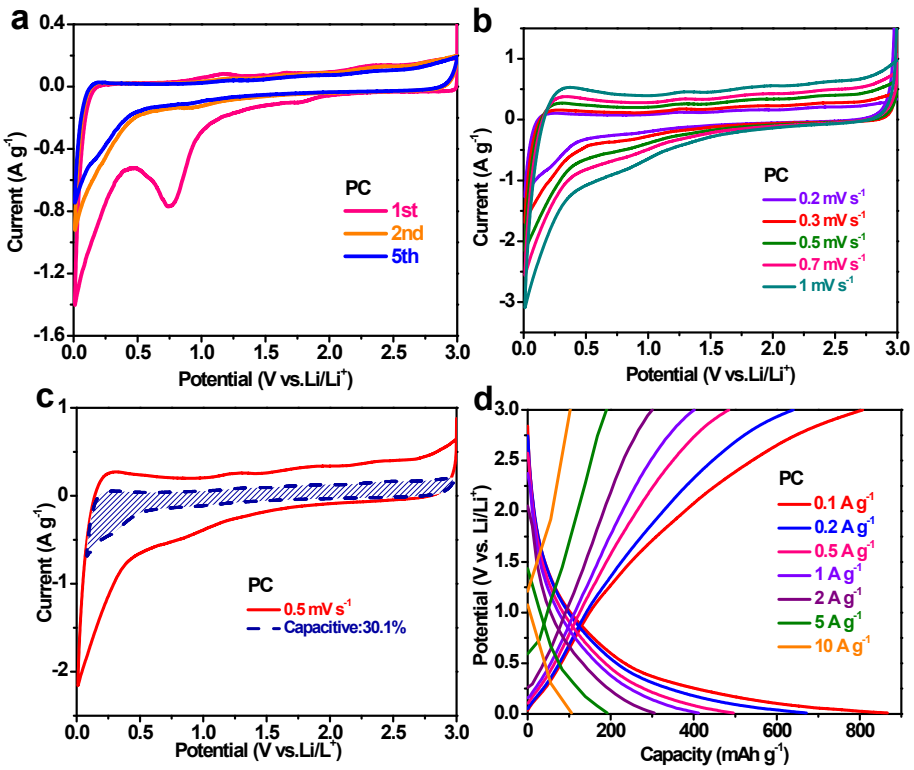

Figure S6. Electrochemical properties of PC tested for lithium-ion battery anodes. (a) CV curves for the first, second, and fifth cycles at the scan rate of 0.1 mV s^{-1}. (b) CV curve at different scan rates, and (c) CV curve at 0.5 mV s^{-1} with shadowed area representing the surface capacitive contribution. (d) Charge-discharge curves at different current densities.

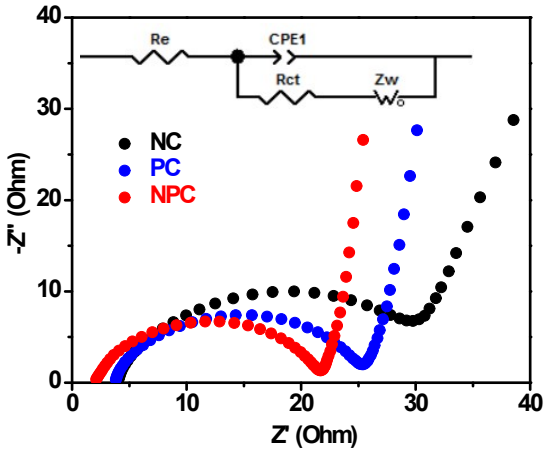

Figure S7. Nyquist plots and equivalent circuit model of all electrodes.

Table S3. Comparison of capacity and cycling stability for N-doped carbon-based LIB-anode with previous reports.

Sample	Voltage window	Capacity	Cyclability	Heteroatom content
NPC (this work)	0.01-3 V	1500-1800 mAh g^{-1} at 0.1A g^{-1}; ~1200 mAh g^{-1} at 0.2 A g^{-1}; ~940 mA h g^{-1} at 0.5 A g^{-1}; ~650 mA h g^{-1} at 2 A g^{-1}; ~369 mAh g^{-1} at 10 A g^{-1};	1475 mAh g^{-1}, 230 cycles (0.1 A g^{-1}) 385 mAh g^{-1}, 2000 cycles (5 A g^{-1}) 301 mAh g^{-1}, 5000 cycles (10 A g^{-1})	N (1.97 at%) O (3.37 at%)
Hierarchical porous N-rich carbon nanospheres[1]	0.01-3 V	1158 mAh g^{-1} at 0.1 A g^{-1}; 907 mA h g^{-1} at 0.5 A g^{-1}; 796 mAh g^{-1} at 1 A g^{-1}; 470 mAh g^{-1} at 5 A g^{-1};	788 mAh g^{-1}, 500 cycles (1 A g^{-1}) 396 mAh g^{-1}, 1000 cycles (5 A g^{-1})	N (17.4 wt%)
N-doped hollow carbon nanospheres[2]	0.01-3 V	1945 mAh g^{-1} at 0.1 A g^{-1}; 1167 mAh g^{-1} at 3.2 A g^{-1};	879 mAh g^{-1}, 1000 cycles (5 A g^{-1})	N (16.6 at%)
N-rich carbon spheres3	0.01-3 V	1038 mAh g^{-1} at 0.1 A g^{-1}; 752 mA h g^{-1} at 0.5 A g^{-1}; 454 mAh g^{-1} at 2 A g^{-1}; 272 mAh g^{-1} at 6 A g^{-1};	1391 mAh g^{-1}, 100 cycles (0.1 A g^{-1}) 638 mAh g^{-1}, 2000 cycles (2 A g^{-1})	N (14.51 %)
Pyrrolic N-enriched carbon fibers[4]	0.005-3 V	842.9 mAh g^{-1} at 0.1 A g^{-1}; 447.6 mA h g^{-1} at 1 A g^{-1}; 282.0 mAh g^{-1} at 5 A g^{-1}; 184.1 mAh g^{-1} at 15 A g^{-1};	789.7 mAh g^{-1}, 500 cycles (1 A g^{-1}) 370.9 mAh g^{-1}, 1000 cycles (5 A g^{-1})	N (3.87 at%)
N-enriching carbon networks[5]	0.01-3 V	1300 mAh g^{-1} at 0.2 A g^{-1}; 770 mA h g^{-1} at 1 A g^{-1}; 360 mAh g^{-1} at 5 A g^{-1}; 280 mAh g^{-1} at 10 A g^{-1};	~600 mAh g^{-1}, 1000 cycles (5 A g^{-1})	N (9.7 at%)
N-doped	0.01-3 V	2163 mAh g^{-1} at 0.1 A g^{-1};	785 mAh g^{-1}, 1000 cycles (5 A g^{-1})	N (25.99

graphene		1790 mA h g^{-1} at 0.2 A g^{-1};		wt%)
analogous		1361 mAh g^{-1} at 0.8 A g^{-1};		
particles[6]		1182 mAh g^{-1} at 1.6 A g^{-1};		
N-doped porous	0.01-3 V	1455 mAh g^{-1} at 0.1 A g^{-1};	~300 mAh g^{-1}, 500 cycles (2 A g^{-1})	N (7.2 wt%)
carbons derived		604-658 mA h g^{-1} at 0.5 A g^{-1};		O (7.4 wt%)
from natural		223-233 mAh g^{-1} at 5 A g^{-1};		
polysaccharide[7]		162-173 mAh g^{-1} at 10 A g^{-1};		
N, O-codoped	0.01-3 V	900-1000 mAh g^{-1} at 0.1 A g^{-1};	~350 mAh g^{-1}, 500 cycles (2 A g^{-1})	N (0.64-0.85
hierarchical		650 mA h g^{-1} at 0.5 A g^{-1};		at%)
porous carbons[8]		220 mAh g^{-1} at 5 A g^{-1};		O (11.4-12.2
		170 mAh g^{-1} at 10 A g^{-1};		at%)

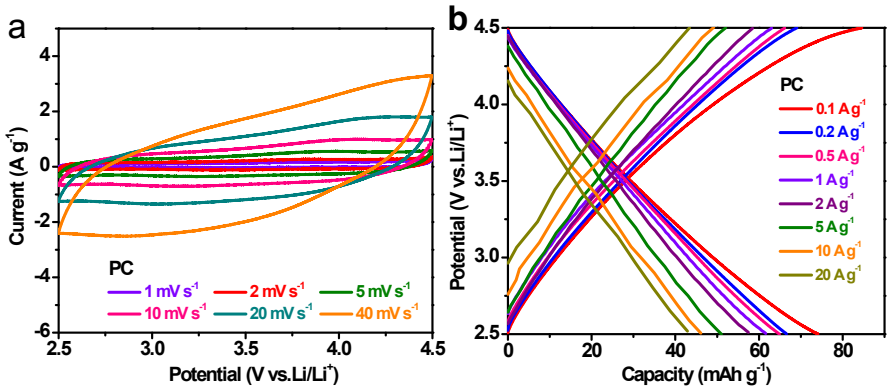

Figure S8. (a) CV curves at different scan rates, and (b) charge-discharge curves at different current densities for PC electrode for lithium-ion battery cathode.

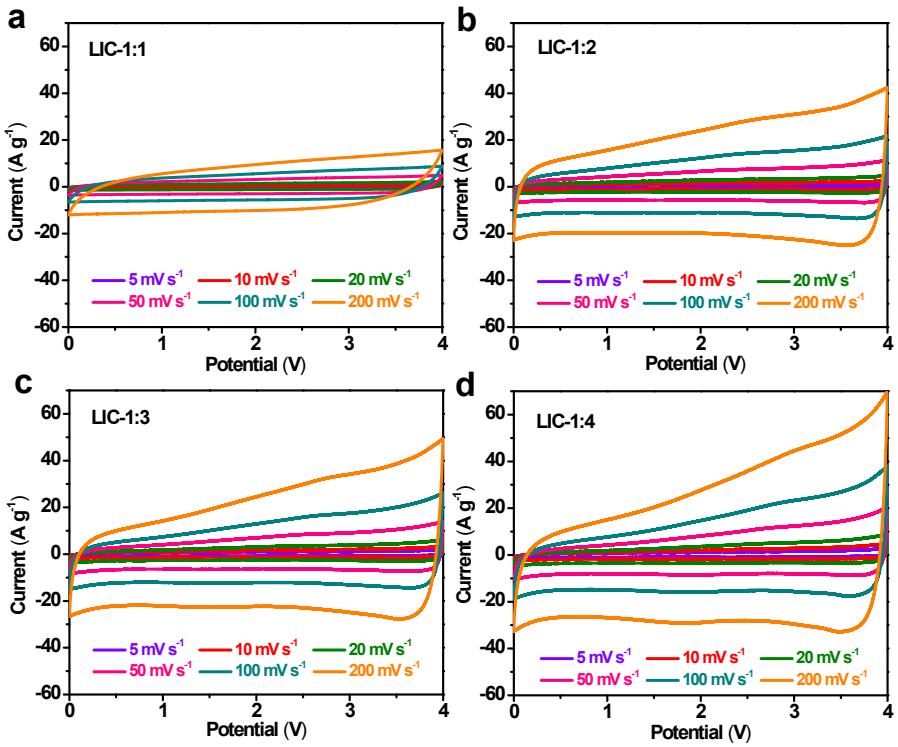

Figure S9. Typical CV curves of the NPC//NPC ACS-LIC at different scan rates for the voltage window of 0-4.0 V.

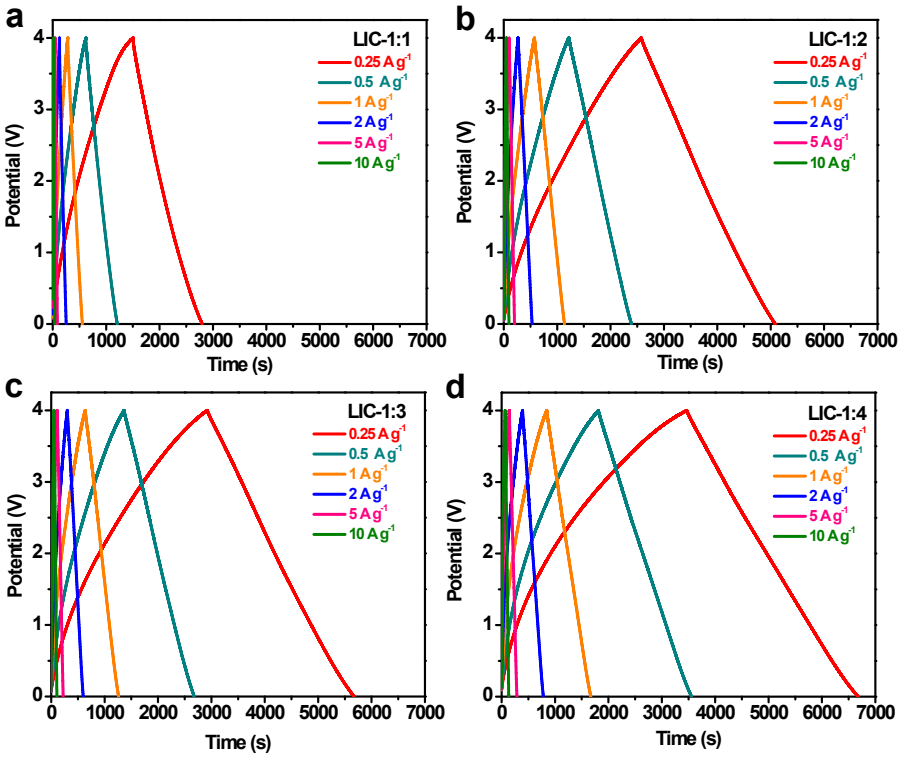

Figure S10. Typical charge-discharge curves of the NPC//NPC ACS-LIC at different current densities of the 0.25-10 A g^{-1} for the voltage window of 0-4.0 V.

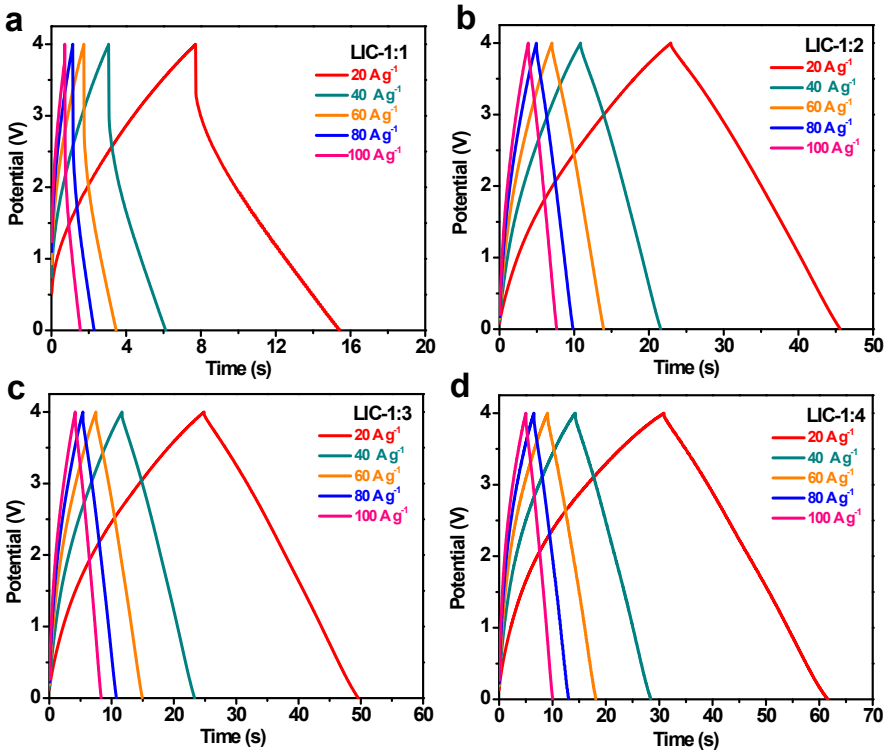

Figure S11. Typical charge-discharge curves of the NPC//NPC ACS-LIC at high current densities of the 20-100 A g^{-1} for the voltage window of 0-4.0 V.

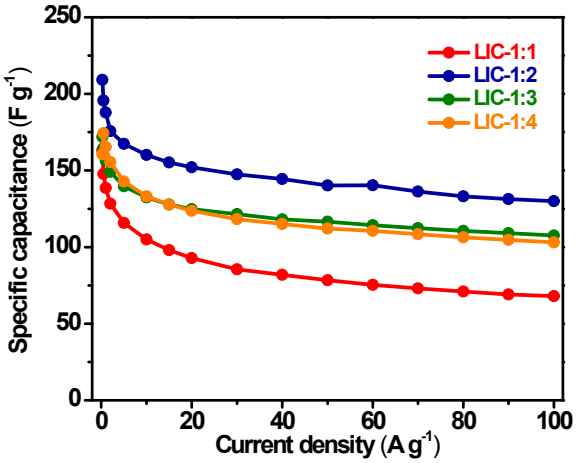

Figure S12. Specific capacitances of the NPC//NPC ACS-LIC at different current densities based on total mass of the both cathode and anode.

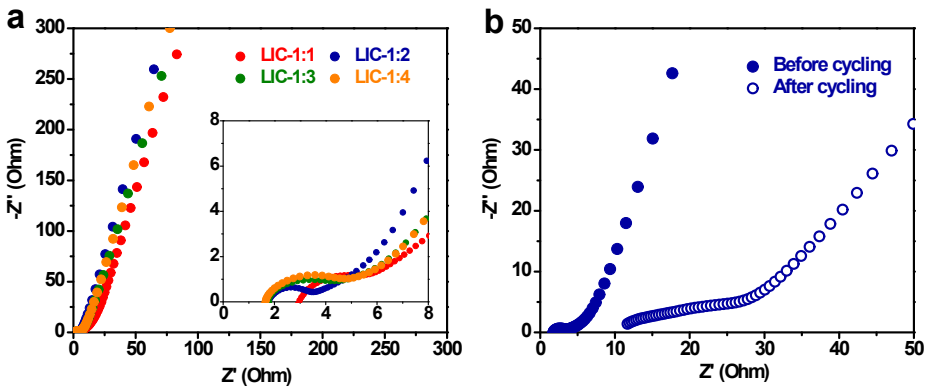

Figure S13. (a) Nyquist plots of the NPC//NPC ACS-LIC, and (b) Nyquist plot for NPC//NPC LIC-1:2 before/after cycling.

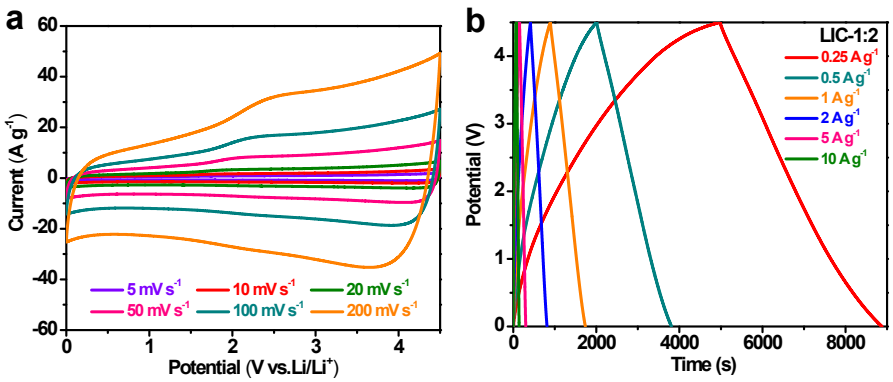

Figure S14. The electrochemical property of the NPC//NPC LIC with anode to cathode mass ratios of 1:2 in the voltage window of 0-4.5 V. (a) CV curves at different scan rates. (b) Charge-discharge curves at different current densities of the 0.25-10 A g^{-1}.

Table S4. Comparison of capacitance and energy density of carbon-based electrodes for supercapacitors in ionic liquid electrolyte.

Sample	Voltage window	Maximum energy	Energy at high power	Cyclability
NPC//NPC (this work)	0-4.0 V	116 Wh kg^{-1} at 167 W kg^{-1}	70 Wh kg^{-1} at 66 kW kg^{-1}	80%, 20000 cycles (10 A g^{-1}) 104.8%, 10000 cycles (2 A g^{-1})
	0-4.5 V	203 Wh kg^{-1} at 187 W kg^{-1}	103 Wh kg^{-1} at 42 kW kg^{-1}	84.6%, 5000 cycles (10 A g^{-1})
BNC//BNC [9]	0.02-4.0 V	133 Wh kg^{-1} at 200 W kg^{-1}	72 Wh kg^{-1} at 22.5 kW kg^{-1}	~104%, 5000 cycles (2 A g^{-1})
	0.02-4.5 V	220 Wh kg^{-1} at 225 W kg^{-1}	104 Wh kg^{-1} at 20 kW kg^{-1}	81%, 5000 cycles (2 A g^{-1})
PHPNC//TiC[10]	0-4.5 V	101.5 Wh kg^{-1} at 450 W kg^{-1}	23.4 Wh kg^{-1} at 67.5 kW kg^{-1}	92%, 5000 cycles at 0-4 V voltage window (2 A g^{-1}) 82%, 5000 cycles (2 A g^{-1})
MnO-C//CNS[11]	1.0-4.0 V	100 Wh kg^{-1} at 83 W kg^{-1}	30 Wh kg^{-1} at 20 kW kg^{-1}	70%, 5000 cycles (5 A g^{-1})
C//SnO_2-C[12]	0.005-4.5 V	110 Wh kg^{-1} at 1 A g^{-1}	-	80%, 2000 cycles (1 A g^{-1})
Fe_3O_4/G//PG[13]	1.0-4.0 V	204 Wh kg^{-1} at 55 W kg^{-1}	122 Wh kg^{-1} at 1000 W kg^{-1}	70%, 1000 cycles (2 A g^{-1})
GDY//AC[14]	2.0-4.0 V	110.7 Wh kg^{-1} at 100.3 W kg^{-1}	95.1 Wh kg^{-1} at 1000.4 W kg^{-1}	94.7%, 1000 cycles (0.2 A g^{-1})
CPIMS//AC[15]	2.0-4.0 V	29.5 Wh kg^{-1} at 356 W kg^{-1}	13.4 Wh kg^{-1} at 7022 W kg^{-1}	97.1%, 1000 cycles (0.5 A g^{-1})
G-LTO//G-SU[16]	0-3.0 V	95 Wh kg^{-1} at 45 W kg^{-1}	32 Wh kg^{-1} at 3000 W kg^{-1}	87%, 500 cycles (15C)
VN-RGO//APDC[17]	0-4.0 V	162 Wh kg^{-1} at 200 W kg^{-1}	64 Wh kg^{-1} at 10 kW kg^{-1}	83%, 1000 cycles (2 A g^{-1})
HDMPC||HDMPC[18]	1.0-4.0 V	106.4 Wh kg^{-1} at 500 W kg^{-1}	10.2 Wh kg^{-1} at 88.8 kW kg^{-1}	88.3%, 8000 cycles (2 A g^{-1})
NPCM//NPCM-A[19]	2.0-4.0V	95.08 Wh kg^{-1} at 300 W kg^{-1}	10.2 Wh kg^{-1} at 15 kW kg^{-1}	80.1%, 5000 cycles (1500 W kg^{-1})

Notes and References

1 L. Ma, R. Chen, Y. Hu, G. Zhu, T. Chen, H. Lu, J. Liang, Z. Tie, Z. Jin and J. Liu, *Nanoscale*, 2016, **8**, 17911-17918.

2 Y. Yang, S. Jin, Z. Zhang, Z. Du, H. Liu, J. Yang, H. Xu and H. Ji, *ACS Applied Materials & Interfaces*, 2017, **9**, 14180-14186.

3 F. Sun, J. Gao, X. Liu, L. Wang, Y. Yang, X. Pi, S. Wu and Y. Qin, *Electrochimica Acta*, 2016, **213**, 626-632.

4 B. He, G. Li, L. Chen, Z. Chen, M. Jing, M. Zhou, N. Zhou, J. Zeng and Z. Hou, *Electrochimica Acta*, 2018, **278**, 106-113.

5 L. Wang, C. Yang, S. Dou, S. Wang, J. Zhang, X. Gao, J. Ma and Y. Yu, *Electrochimica Acta*, 2016, **219**, 592-603.

6 F. Zheng, Y. Yang and Q. Chen, *Nature Communications*, 2014, **5**, 5261.

7 Y. Cui, H. Wang, X. Xu, Y. Lv, J. Shi, W. Liu, S. Chen and X. Wang, *Sustainable Energy & Fuels*, 2018, **2**, 381-391.

8 W. Yu, H. Wang, S. Liu, N. Mao, X. Liu, J. Shi, W. Liu, S. Chen and X. Wang, *Journal of Materials Chemistry A*, 2016, **4**, 5973-5983.

9 Q. Xia, H. Yang, M. Wang, M. Yang, Q. Guo, L. Wan, H. Xia and Y. Yu, *Advanced Energy Materials*, 2017, **7**.

10 H. Wang, Y. Zhang, H. Ang, Y. Zhang, H. T. Tan, Y. Zhang, Y. Guo, J. B. Franklin, X. L. Wu, M. Srinivasan, H. J. Fan and Q. Yan, *Advanced Functional Materials*, 2016, **26**, 3082-3093.

11 Y. Zhao, Y. Cui, J. Shi, W. Liu, Z. Shi, S. Chen, X. Wang and H. Wang, *Journal of Materials Chemistry A*, 2017, **5**, 15243-15252.

12 W.-H. Qu, F. Han, A.-H. Lu, C. Xing, M. Qiao and W.-C. Li, *Journal of Materials Chemistry A*, 2014, **2**, 6549.

13 F. Zhang, T. Zhang, X. Yang, L. Zhang, K. Leng, Y. Huang and Y. Chen, *Energy & Environmental Science*, 2013, **6**, 1623.

14 H. Du, H. Yang, C. Huang, J. He, H. Liu and Y. Li, *Nano Energy*, 2016, **22**, 615-622.

15 X. Han, P. Han, J. Yao, S. Zhang, X. Cao, J. Xiong, J. Zhang and G. Cui, *Electrochimica Acta*, 2016, **196**, 603-610.

16 K. Leng, F. Zhang, L. Zhang, T. Zhang, Y. Wu, Y. Lu, Y. Huang and Y. Chen, *Nano Research*, 2013, **6**, 581-592.

17 R. Wang, J. Lang, P. Zhang, Z. Lin and X. Yan, *Advanced Functional Materials*, 2015, **25**, 2270-2278.

18 J. Niu, R. Shao, M. Liu, J. Liang, Z. Zhang, M. Dou, Y. Huang and F. Wang, *Energy Storage Materials*, 2018, **12**, 145-152.

19 J. Jiang, P. Nie, B. Ding, Y. Zhang, G. Xu, L. Wu, H. Dou and X. Zhang, *Journal of Materials Chemistry A*, 2017, **5**, 23283-23291.